Turkish Journal of Electrical Engineering & Computer Sciences

http://journals.tubitak.gov.tr/elektrik/

Research Article

Turk J Elec Eng & Comp Sci
(2018) 26: 3207 – 3223

doi:10.3906/elk-1711-113

Attenuating saturated-regulator operation effect of brushless DC motors through genetic-based fuzzy logic estimator

Emre ÇELİK[1,*], **Nihat ÖZTÜRK**[2]

[1]Department of Electrical and Electronics Engineering, Faculty of Engineering, Düzce University, Düzce, Turkey
[2]Department of Electrical and Electronics Engineering, Faculty of Technology, Gazi University, Ankara, Turkey

Received: 13.11.2017 • **Accepted/Published Online:** 30.08.2018 • **Final Version:** 29.11.2018

Abstract: As brushless DC motor (BLDCM) speed approaches base speed, current regulators gradually saturate and lose their ability to perform their regulating task, which causes a dramatic fall in the phase currents and motor power. To control the current to a greater extent and avoid power decline, a new reference current generation technique based on a simple fuzzy logic estimator (FLE) is introduced in this paper. According to motor speed and current command, the developed FLE decides the proper commutation angle α, which is the angle relative to normal commutation instant used for setting the current slew rate during commutation. In this sense, current references are obtained with the same slew rates of commutated phases all the time, ensuring the noncommutation phase current is constant. The validity of the study is widely verified using DSP of TMS320F28335 and it is concluded that promising performance and simplicity are important advantages of our proposal that render it convenient for a BLDCM drive system that requires boosted power in high-speed ranges.

Key words: Brushless DC motor, commutation angle, genetic algorithm, fuzzy logic estimator, saturated-regulator operation

1. Introduction

Brushless DC motors (BLDCMs) offer many advantages such as high power density, high efficiency, low rotor inertia, low maintenance, reliability, and low electromagnetic interference problems [1–3]. Compared with their sinusoidal counterpart, often referred to as a permanent magnet synchronous motor (PMSM), BLDCMs allow some important system and operational simplifications while developing relatively higher power density [4,5]. However, the decrease of output power of such electrical machines during high-speed operation is a major obstacle to achieve higher performance.

At very high speeds beyond the rated/base speed, the inverter without proper control fails to inject current into the motor as the back emf voltage can reach a value close to or greater than that of the power inverter. When the motor is required to operate in such a condition, flux weakening (FW) is an indispensable requirement that opposes the emf by generating a demagnetizing current component I_d that weakens the air gap flux. This is realized by advancing the phase angle of the currents with reference to the back emf. There are many studies that address the issue of FW operation from various aspects [6–13]. As already emphasized, the conventional FW method has severe disadvantages such that it leads to more power losses in the motor and inverter as well as has the risk of irreversible demagnetization of the permanent magnets [6–10]. Moreover,

*Correspondence: emrecelik@duzce.edu.tr

the method exhibits significant torque ripple. Combined by a phase-advance technique, a dual-mode inverter controller was presented in [11] to offer a wide constant power speed range for BLDCM. As expressed, back-to-back thyristors used in the AC-link block the conduction of antiparallel diodes, thereby increasing the net torque and power. However, this is accompanied by significant increases in ripple components of output motor power. In [12,13], FW was obtained by switching the windings in the machine to extend the speed range of PMSMs. In the study, two current-regulated voltage source inverters are used to control the machine. Though the constant torque region is extended, the drive system has a highly complex structure. As a result of our literature review, it is noticed that there are no published studies similar to our proposal that can be taken as benchmark methods for comparison. The birth of this work is based on the idea that instead of advancing the current relative to the back emf to raise the speed in the constant power region, we aim at constructing quasitrapezoidal-like current references in order to maintain the current closer to its commanded value while in phase with the back emf, which therefore increases the power production ($e \times i$) in high-speed ranges. Since the torque is defined as the ratio of motor output power to rotational speed, it can be kept at a constant level as speed increases. In this way, the constant torque region of the motor is widened to higher speeds without leading to the severe power ripple present in FW-based techniques owing to keeping the phase current and back emf in phase. This forms another important feature of our proposal since it ensures operation at maximum torque per amp. We would like to highlight that the extent of operation at higher speeds using the presented technique is limited with a region not wider than in the presence of FW.

Fuzzy logic (FL) theory essentially deals with uncertainty and offers promising performance when the input data are vague and the mathematical representation of a system is complex, unknown, or deficient [14]. It is one of the most adopted theories to control nonlinear and complex plants [15]. FL modeling refers to the process in which a dynamic system is modeled in the form of fuzzy rules and their corresponding membership functions [16]. It may not be always simple to construct a fuzzy system, as there are many parameters to be identified. Besides, since the design is traditionally performed by trial and error from experience and knowledge of a skilled operator, correct application of such information is substantial. Moreover, if there is limited or unavailable operator knowledge, the design process may either become tedious and time-consuming, or even may not be possible. To cope with these problems, cooperation with evolutionary algorithms should be made for acquiring fuzzy design parameters. Of these algorithms, genetic algorithms (GAs) are derived from biological nature and they have been widely used to solve a vast number of optimization problems [17–20]. Although extensive research has been paid to neuro-fuzzy models and adaptive neuro-fuzzy inference system (ANFIS) models, they may be classified as "medium" in complexity in comparison with FL and should be adopted when the use of them justifies the cost and complexity [21]. In the presence of the BLDCM drive, which is famous for its cost and simplicity advantages, they would not be applicable. Contrary to conventional FL, where membership degree is a crisp number in the range [0, 1], a type-2 FL system (T2FLS) is characterized by three-dimensional fuzzy membership functions and has an extra type-reduction process [22,23]. Though generally more robust as well as achieving better performance against uncertainties, T2FLS is not easy to code and leads to increased workload for the microprocessor.

Encouraged by the desire of improving poor current regulation during saturated-regulator operation of a BLDCM, the authors of this article have proposed a new reference current generation mechanism on the basis of equal slew rates of commutated phases during commutation. In this mechanism, the slew rate of the phase current is made adaptive to motor speed and current command, and is set by a control parameter denoted as commutation angle α. By considering the computational and simplicity effectiveness of a FL system over the

above-mentioned approaches, a FL-based estimator (FLE) is preferred in this paper to acquire the value of α from zero to maximum motor speed depending on the motor speed and current command. After three-phase current references are generated using rotor position, current command, and commutation angle, a standard hysteresis current controller is used for regulating the current within the motor winding. Moreover, in order to determine the FLE's rule base effectively, an offline optimization process is realized by deploying a GA. Several experiments based on DSP of TMS320F28335 are provided, which confirm that our proposal has promising performance above base speed. These results are also compared with those obtained by a classical drive system. We realize that our proposal offers important advantages such as superior performance and simplicity, which are concerns of practice.

2. Mathematical model and classical three-phase drive system of BLDCM

In a short form, the BLDCM model is provided in this section first. For this, the motor model and conventions adopted in this paper are shown in Figure 1 as well as the machine ideal trapezoidal back emf waveforms and rectangular stator currents.

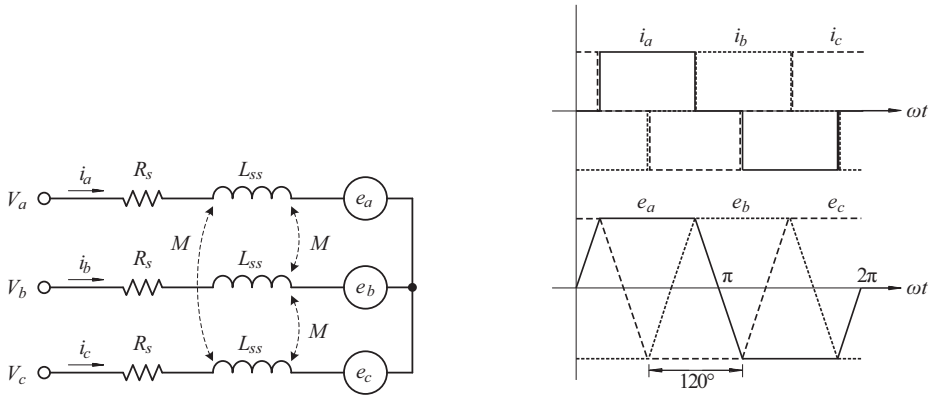

Figure 1. Typical schematics of BLDCM: (a) three-phase equivalent circuit, (b) ideal currents and back emf wave shapes.

The stator voltage equation of the BLDCM is expressed in a three-phase plane as:

$$\begin{bmatrix} V_a \\ V_b \\ V_c \end{bmatrix} = \begin{bmatrix} R_s & 0 & 0 \\ 0 & R_s & 0 \\ 0 & 0 & R_s \end{bmatrix} \begin{bmatrix} i_a \\ i_b \\ i_c \end{bmatrix} + \begin{bmatrix} L_{ss}-M & 0 & 0 \\ 0 & L_{ss}-M & 0 \\ 0 & 0 & L_{ss}-M \end{bmatrix} \frac{d}{dt} \begin{bmatrix} i_a \\ i_b \\ i_c \end{bmatrix} + \begin{bmatrix} e_a \\ e_b \\ e_c \end{bmatrix}, \quad (1)$$

where V_a, V_b, V_c are the phase voltages; i_a, i_b, i_c are the phase currents; e_a, e_b, e_c are the electromotive forces; and R_s is the stator winding resistance per phase. In Eq. (1), the expression $L_{ss}-M$ is termed as the motor synchronous inductance L_s and is equal to:

$$L_s = L_{ss} - M = L_l + L_{ms} - \left(-\frac{1}{2}L_{ms}\right) = L_l + \frac{3}{2}L_{ms}. \quad (2)$$

In Eq. (2), L_{ss} is the total phase inductance composed of winding leakage L_l and self-inductance L_{ms}, and M represents the mutual inductance between the motor adjacent phases. The electromagnetic torque T_e is given

by:

$$T_e = \frac{p}{2}\frac{e_a i_a + e_b i_b + e_c i_c}{\omega_r}, \tag{3}$$

where p is the pole number and ω_r is the electrical rotor speed in rad s^{-1}. Finally, we can derive the rotor speed equation in state-space form as:

$$\frac{d}{dt}\omega_r = \frac{p}{2}\left(T_e - T_L - B\left(\frac{2}{p}\right)\omega_r\right)\Big/ J. \tag{4}$$

In Eq. (4), T_L is the load torque, and J and B are the coefficients of inertia and viscous friction torque of the rotating rotor, respectively.

In a classical three-phase BLDCM drive system, motor currents are controlled individually, which requires that two or three current sensors be placed in the AC-link to sense each of the individual phase currents. Given the structure of this kind of current control and the possible six switch states in Figure 2, ideal rectangular current references with 120°duration each half cycle are generated as a function of rotor position θ_r and current command I, and hysteresis current controllers generate switch signals by comparing the current references $i^*_{a,b,c}$ with the sensed ones $i_{a,b,c}$. Thus, stator currents are forced to strictly follow the references by the proper three power switches at all times.

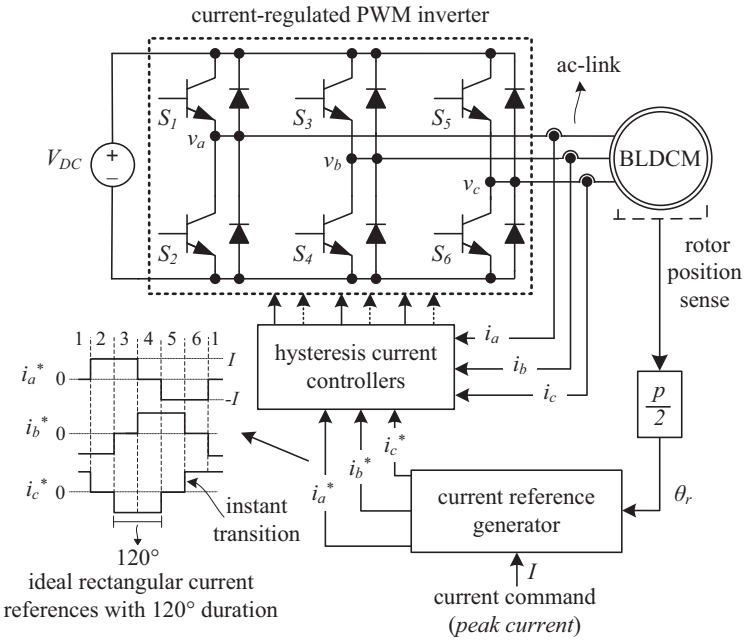

switch states

switches	1	2	3	4	5	6
S_1	NA	1	1	NA	0	0
S_2	NA	0	0	NA	1	1
S_3	0	0	NA	1	1	NA
S_4	1	1	NA	0	0	NA
S_5	1	NA	0	0	NA	1
S_6	0	NA	1	1	NA	0

1 = Switch closed 0 = Switch open
NA = dependent on current value at zero current reference

Figure 2. Schematic of classical BLDCM drive with AC-link current sensing and possible switch states.

However, since the instant transition of rectangular references makes them difficult to be followed by the stator currents during high-speed operation, we consider a new reference current waveform that possesses no discontinuity and changes level in a finite time. With this aim, a new parameter called the commutation angle α is integrated into the current reference generation mechanism in this article, as depicted in Figure 3. α is a critical parameter that corresponds to current slew rate during commutation. Its value is estimated online by the developed FLE depending on the amplitude of rotor speed ω_m and current command I because the current

controllability in motor winding is restricted by these two quantities. ω_m and I are fed to the FLE as inputs through the normalizing gains K_1 and K_2, which are equal to $1/\omega_{max}$ and $1/I_{\max}$, respectively, and there is no gain on the output of FLE for α. As highlighted by the dashed ellipse shape in Figure 3, current references may take the form of quasitrapezoidal waves, which do not exert instant transitions during commutation. From this perspective, the paper concentrates on optimizing current slew rates of the reference currents to increase drive performance under high-speed saturated-regulator excitation.

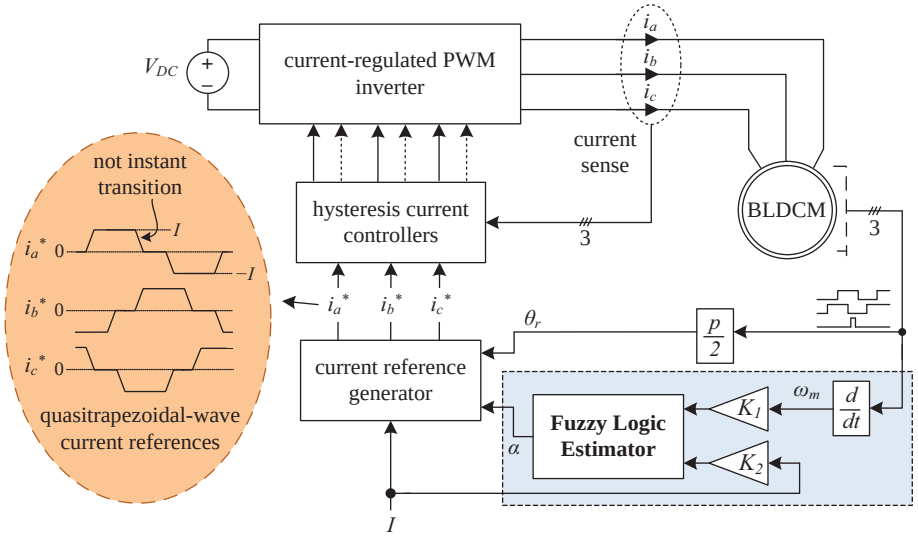

Figure 3. Schematic of the proposed three-phase BLDCM drive.

The main idea of the paper lies in constructing reference currents to be of a waveform similar to quasi-trapezoidal as speed and current command increase while trying to maintain the current in phase with its back emf to get the highest torque-current ratio. As clearly seen in Figure 4, instead of commanding reference currents to perform instant transitions, we force the adjacent phases to start commutating α degrees before the normal commutation instant while finishing commutation α degrees after the normal commutation instant, which yields a commutation period of $\beta = 2\alpha$ and reference current slew rates equal to $m = \mp I/2\alpha$. Such a change in reference current shaping is made so that the rising phase current is given a certain time (proportional to α, in this case) to build up to its required value before its back emf reaches its maximum value and the same time is given to the falling phase current to vanish gradually. This helps increase current tracking capability of the inverter at high speed operation, which forms our main contribution. It is also worth highlighting that during commutation time, slew rate magnitudes of commutated phases are kept the same with opposite sign all the time, which favorably ensures constant noncommutation phase current that is also the current responsible for torque production of the BLDCM in the commutation process. This can be expressed theoretically in Figure 4 as $m_a = 0$ when making $|m_b| = |m_c|$.

If a point is reached where the actual current is no longer able to track its reference owing to possible increase in ω_m and/or I, then the FLE begins to gradually increase α that again allows the phase current to follow the reference. In another case, the FLE reduces α to its required value. Notice that the relation of α with regard to ω_m and I need not be known using any mathematical formulas in the article. The analytic expressions of the reference currents for each zone are tabulated in Table 1.

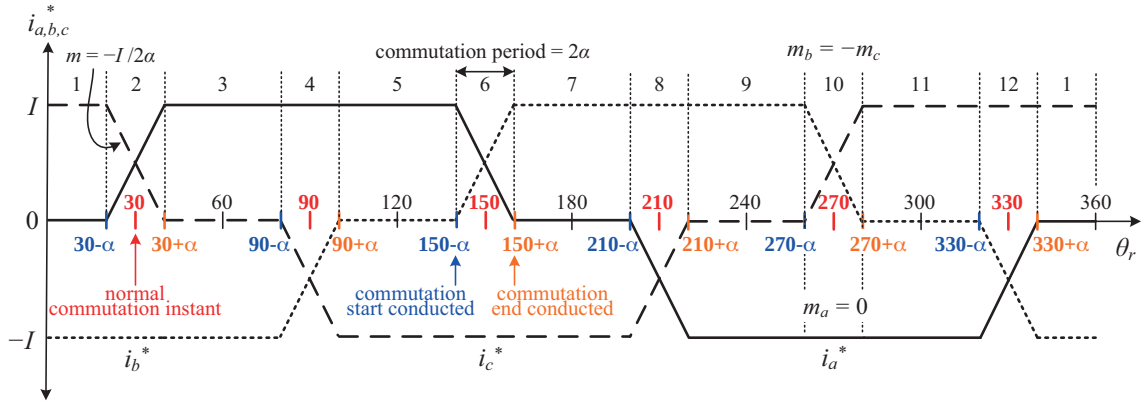

Figure 4. Quasitrapezoidal current references with the same slew rates during commutation.

Table 1. Analytic expressions of the reference currents.

Zone	i_a^*	i_b^*	i_c^*
1	0	$-I$	I
2	$m(\theta_r - (30 - \alpha))$	$-I$	$I - m(\theta_r - (30 - \alpha))$
3	I	$-I$	0
4	I	$-I + m(\theta_r - (90 - \alpha))$	$-m(\theta_r - (90 - \alpha))$
5	I	0	$-I$
6	$I - m(\theta_r - (150 - \alpha))$	$m(\theta_r - (150 - \alpha))$	$-I$
7	0	I	$-I$
8	$-m(\theta_r - (210 - \alpha))$	I	$-I + m(\theta_r - (210 - \alpha))$
9	$-I$	I	0
10	$-I$	$I - m(\theta_r - (270 - \alpha))$	$m(\theta_r - (270 - \alpha))$
11	$-I$	0	I
12	$-I + m(\theta_r - (330 - \alpha))$	$-m(\theta_r - (330 - \alpha))$	I

3. Structure of the FLE

The input variables of the developed FLE are mechanical speed ω_m and current setpoint I. The commutation angle α is assigned as the output variable. Five symmetrical triangle membership functions are structured for both ω_m and I. In order to reduce the computational burden of the defuzzification process, five membership functions of singleton-type are selected for the output fuzzy variable. As shown in Figure 5, input variables are in the range of [–1, 1], and the output variable is in the range of $[\pi/180,\ 30\pi/180]$.

For the fuzzy inference system, which is the heart of a fuzzy system, the common min-max (or and-or) method is selected, and defuzzification is performed using the weighted-average method. The FLE's rule base is effectively constructed by using a GA in this study, rather than adopting a trial and error method, which uses expert knowledge and experience if available.

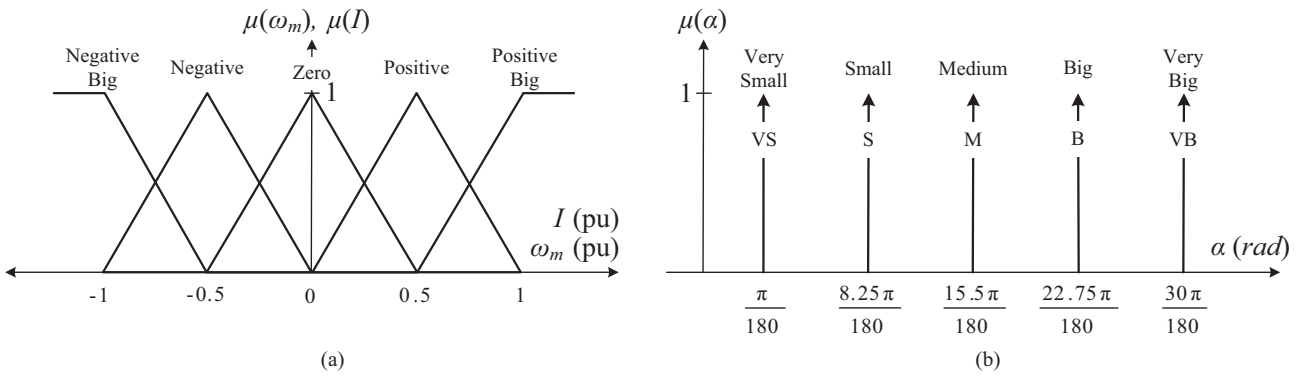

Figure 5. Membership functions defined for (a) ω_m, I (b) α.

3.1. Preparation of the rule base for optimization by the GA

As the construction of the rule base plays an important role in the performance and nonlinearity characteristics of a fuzzy system, this article attempts to apply a GA to acquire the FLE's rule base effectively without need for human assistance. Before beginning the optimization with the GA, some characteristic parameters are required for construction of the rule base. As five fuzzy sets are defined for the input variables, the rule base consists of a total of $5 \times 5 = 25$ fuzzy rules, which yields a 25-D optimization problem highly difficult to be solved. Thus, we have made some useful simplifications over the rule base structure to facilitate the optimization by reducing the number of required fuzzy rules. The rule base can be considered as a table with 25 cells as in Figure 6. The rules on the z-axis are adopted equal while the ones on the x- and y-axes are symmetric with the y- and x-axes, respectively. Other rules out of these axes are symmetric with origin, thereby reducing the number of parameters to 11 as $s_1 s_2, \ldots, s_{11}$, each of which corresponds to an output membership function.

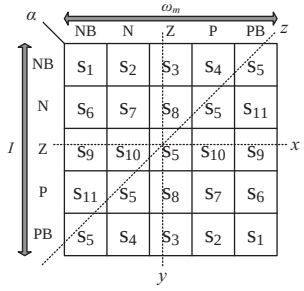

Figure 6. Preparation of rule base for the optimization.

As a result, eleven characteristic parameters $s_1 s_2, \ldots, s_{11}$ are defined to form a chromosome in the GA by $S = [s_1, s_2, \ldots, s_{11}]$. These members or genes in an individual are represented by real numbers as VS = 1, S = 2, M = 3, B = 4, and VB = 5. If the number of chromosomes in a population is N, then the population dimension is $N \times 11$.

3.2. Definition of the multiobjective performance index

A performance index is a quantitative measure that decides which chromosomes will survive into the next generation [24]. In this study, as it is highly desirable for the phase currents to track the produced reference currents as much as possible, deviation of the phase currents from the references are calculated by the integral

absolute error (IAE). In addition, the value of current command I is added to the performance index to fulfill the second objective for maintaining operation with minimum value of α in all operating conditions. Thus, the resulting multiobjective performance index is given by:

$$P = \gamma \int_0^{t_{sim}} |i_x^* - i_x| \, dt + \delta I. \tag{5}$$

The optimization of the rule base consists of minimizing the performance index P, where i_x^* and i_x are reference and actual phase current with subscript x being the phase indices. t_{sim} is simulation time, and the significance of each term in Eq. (5) is determined by the weight factors γ and δ. In order to attain the desired performance, it is up to the user to set the weight factors appropriately. For the current study, selections are $\gamma = 0.7$ and $\delta = 0.3$. An increase in γ will lead to some improvement in the corresponding feature at the cost of diminishing other features.

3.3. Rule base derivation through offline GA optimization

This paper uses the offline optimization technique, using the GA as the effective optimization means. GA incorporation is devoted to automate the process of defining rule base parameters by a suitable simulation model while the other FLE parameters are fixed. For this, we first prepare ANSI C-based software that simulates the operation of the BLDCM drive system. The initial population contains 40 randomly generated chromosomes; each chromosome has eleven rule base characteristic parameters. Each chromosome is fed into the BLDCM drive system to make simulation for a time horizon t_{sim} and assess the chromosome performance under a certain speed reference and load torque. Then a fitness value is computed for each chromosome using Eq. (5). During optimization, motor reference speed and load torque are assumed to vary in the range covered by the motor nameplate. In this way, a total of 60 different operating conditions are obtained. The final cost F regarding each chromosome is equal to the mean of these 60 costs, which is mathematically given by

$$F = \left(\sum_{i=1}^{OC} P_i \right) \Big/ OC, \tag{6}$$

where OC is the number of operating conditions that are used for simulation in each objective function calculation. If the current iteration does not reach the maximum iteration number, the population is sorted from the fittest chromosome to the worst one. As our goal is to minimize Eq. (6), the chromosome with the lowest value of Eq. (6) will stand in the first row of the population. Using a discard rate of p_d, $p_d \times N_{pop}$ members located at the end of the population are discarded from the population, and the qualified remainder become potential parents for new generations. After selecting the parents by rank-based roulette wheel selection mechanism, crossover is applied to the selected parents to produce new members that replace the discarded ones. Finally, mutation is executed depending on the mutation rate p_m in each iteration to introduce random changes within the algorithm. The following detailed flowchart of the GA implementation gives a better picture of the above explanation.

Table 2 reports the GA parameters selected via many successive trials.

Using the GA parameters in Table 2, an optimization program is run subsequently five times under random initial circumstances, and the convergence profile of the *best* chromosome in each case is shown in Figure 8a for the first 20 iterations. As seen, all curves start from different points owing to the random

Table 2. GA parameters.

Parameters	Methods/Values	Parameters	Methods/values
Population size (N_{pop})	40	Crossover technique	Uniform
Chromosome length (l)	11	Mutation rate (p_m)	0.5
Maximum generation	3000	Discard rate (p_d)	0.625
Natural selection	Rank-based roulette wheel	Performance criterion (P)	Eq. (5)

population at iteration 1, and after an initial sharp drop, GA converges to an F value of about 1.505 in only 18 iterations, then continues to search for better results around this point. Encouraging convergence behavior of the proposed GA may be perceived from this figure. The obtained rule base at the end of the optimization is also given in Figure 8b. This rule base is used in DSP for practical implementation in the rest of the paper.

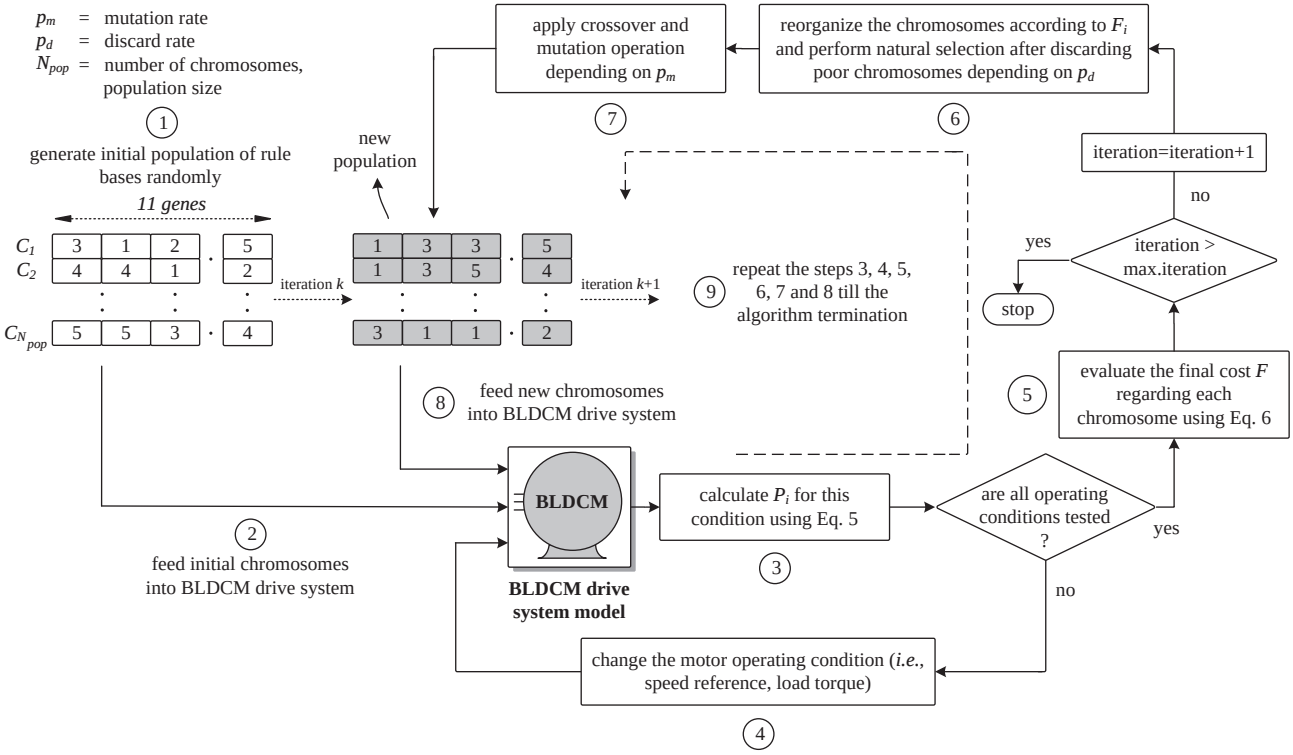

Figure 7. The detailed flowchart of the GA implementation.

4. Experimental verification

In order to confirm the applicability and superior performance of the presented method over the eclassical method, experiments are performed by a 500-W 8-pole BLDCM whose parameters are shown in Table 3. The whole control algorithm is written using the C language in the F28335 eZdsp CCStudio environment, an important portion of which is provided in the Appendix to give birth to new design approaches in the concerned field.

In Figure 9, motor currents are measured by the LA 55-P current transducers and transferred to the DSP along with the rotor position knowledge, which is obtained by a built-in incremental encoder of 2500 ppr.

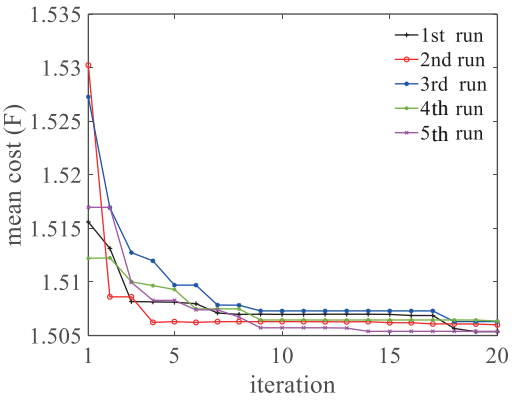

(a)

α \ ω_m	NB	N	Z	P	PB
NB	VB	S	VS	VB	S
N	B	VS	VS	S	M
Z	S	VS	S	VS	S
P	M	S	VS	VS	B
PB	S	VB	VS	S	VB

I

(b)

Figure 8. GA-based optimization results: (a) convergence profiles obtained by five subsequent random runs, (b) optimized rule base.

Table 3. BLDCM parameters.

Features	Values	Features	Values
DC-link voltage	200	Resistance per phase, R_s	2 Ω
Number of poles	8	Inductance, L_s	3.5 mH
Base speed	2000 rpm	Flux linkage constant, λ_f	0.0857 Vs/rad
Rated power	500 W	Moment of inertia, J	5.69 $\times 10^{-5}$ kg m^2
Rated rms current	5 A	Friction coefficient, B	10^{-4} kg s/rad

Rotor position signals and gate signals of the inverter are isolated from the hardware setup to avoid undesirable noise using high speed 6N137 optocouplers. A snubber capacitor of Alcon KP-6 0.068µF/2000V is connected in parallel with each arm of the inverter with a filter capacitor of Epcos 4700 μF 450V at its input. Ixys IGBTs of IXGH48N60C3D1 are chosen as power switches, which are driven through gate drive circuitry where integrated electronic components M57145L-01 and M57959AL are used to transform DSP gate signals into the signals with which IGBTs can operate. In DSP, hysteresis current bandwidth is set to 0.23 A, motor speed is calculated at every 10 ms, and the interrupt routines for the FLE and 12-bit A/D converter are executed with the period of 200 Hz and 75 kHz, respectively. A dead time of 7 µs is included between the complementary gate signals for the power switches of the same inverter leg. A DC generator is coupled to the BLDCM to apply external torque at the motor shaft.

Figure 10 shows the test bench of the shaft coupling of both machines, in addition to control and power circuitry of the concerned drive system. Phase current waveform is collected and viewed by a Yokogawa DLM4038 oscilloscope.

Initially, low-speed performances of the methods are evaluated at a speed and current command of 1000 rpm, 3 A, where the oscilloscope scale is set to 5 A/div and 2 ms/div. It is clear from Figure 11 that below base speed, motor currents are satisfactorily tracking the rectangular references. Under this condition, the commutation angle generated by the FLE is 0.008 rad. Since it is that much smaller, motor current in the presented technique is almost in the form of rectangular, similar to that in the classical approach.

To establish operation with saturated-current regulators, subsequent experiments are carried out at a speed of 1.625 times base speed (3250 rpm), with the current commands of 4, 5, 6, and 7 A. At 3250 rpm, the

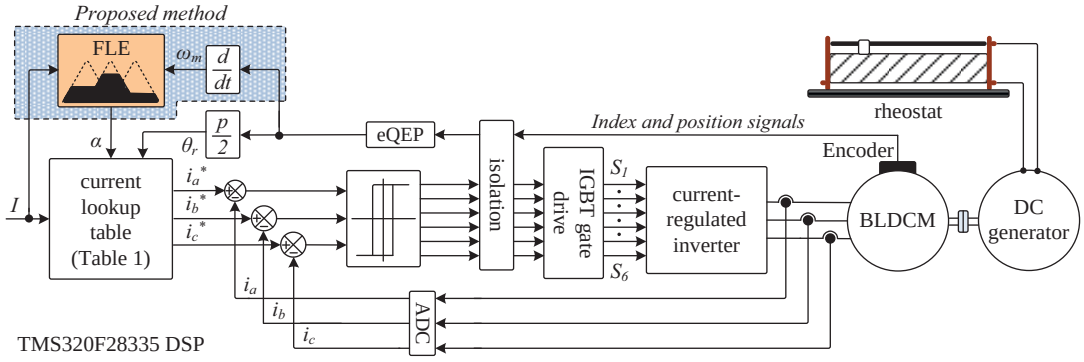

Figure 9. Hardware block diagram of the presented control scheme.

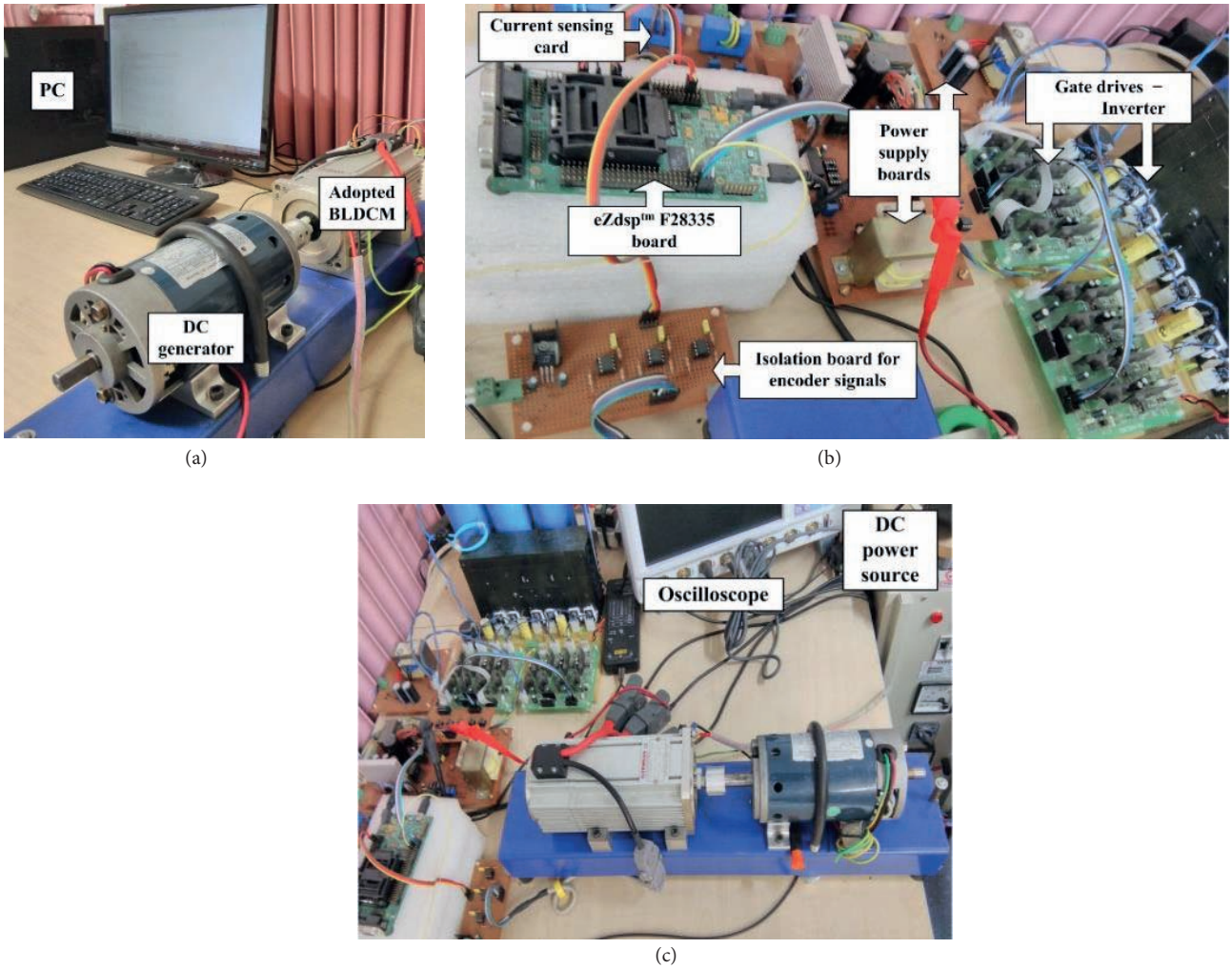

Figure 10. The DSP-based experimental setup: (a) test bench, (b) control and power circuitry, (c) panoramic view.

peak value of motor emf exceeds the inverter DC-link voltage. At this time, the time scale of the oscilloscope is decreased to 1 ms/div. The dashed blue lines standing for the reference currents are provided to show how the current deviation from its rectangular reference could be considerable when the current regulators become

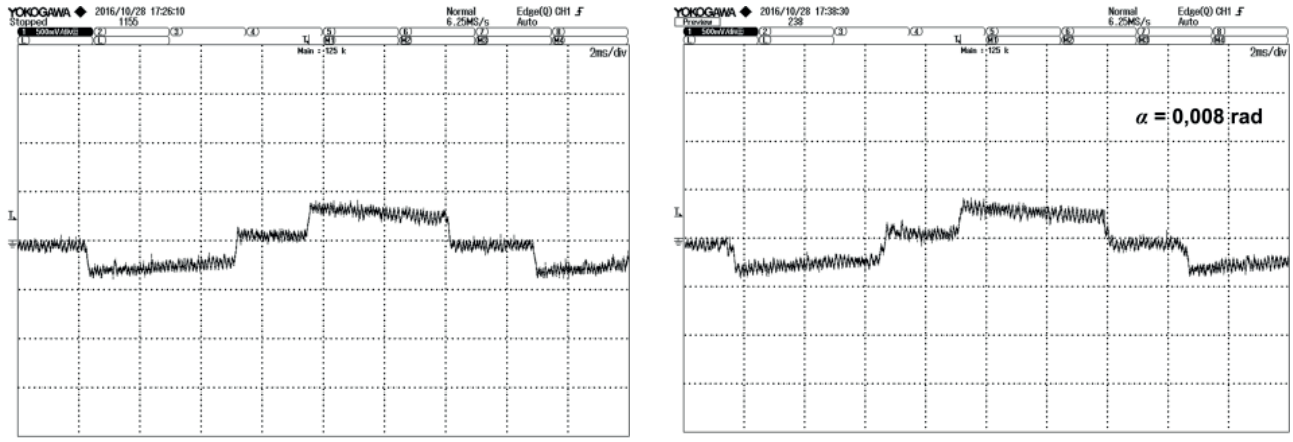

(a) (b)

Figure 11. Experimental results of phase a motor current waveforms at 1000 rpm and $I = 3$ A: (a) classical, (b) presented.

saturated. Classical results are displayed on the left side of the paper, and the opposite side shows those based on our proposal.

It is apparent from Figure 12 that the inverter controlled by the classical method fails to force the commanded current into the motor phase. Due to the tendency of freewheeling diodes to conduct at high speed, two-phase operation can no longer be maintained, which means that the third-phase current is hardly kept at zero between the commutation intervals. It is also observed that increasing the current command gives rise to more distortion in the current waveform. As both current wave shape and peak current are not at the desired level, it results in ripple content along with rapid decline in output motor power. Comparing these results to those with the presented technique, at first glance, we see that for any of the current commands, the proposed approach is clearly less influenced by the high-speed operation in that the phase current waveforms now seem more regular and much closer to the generated quasitrapezoidal references. For each current command value, the FLE automatically sets the required value of α in order to avoid poor current regulation through the inverter saturation. Starting from 0.343 rad, α reaches 0.405 rad when $I = 7$A. Considering Figures 11 and 12, we can conclude that α is varied proportionally to ω_m and I; thus, any increase in ω_m or I reflects itself as an increase in α. In addition, since output power, following the electromagnetic torque, is closely related to phase current, we can approximately estimate the waveform of output motor power from the phase current shape, which would appear to be, of course, more smooth in the presented technique than in its classical counterpart. This is also an appealing feature of the study compared to techniques adopting FW, which suffer from significant power ripple.

To further demonstrate the validity of the presented method, input DC-link power and output generator power of the drive system are measured and the results are shown in Figures 13a and 13b. It is found that the greatest output power improvement is 60%, which is achieved when the speed and current command are 3250 rpm and 5 A, respectively. Note that these output power values are not a true motor shaft power. Generator efficiency should be incorporated to obtain the motor output power. Taking the generator efficiency as 0.75, we can then calculate the output motor power as $440 \div 0.75 = 586.7$ W, which yields a power of 1.17 times more than is delivered at base speed. This result shows that the presented technique enables production of more power than the rated power above base speed, unlike the classical method. No improvement is achieved

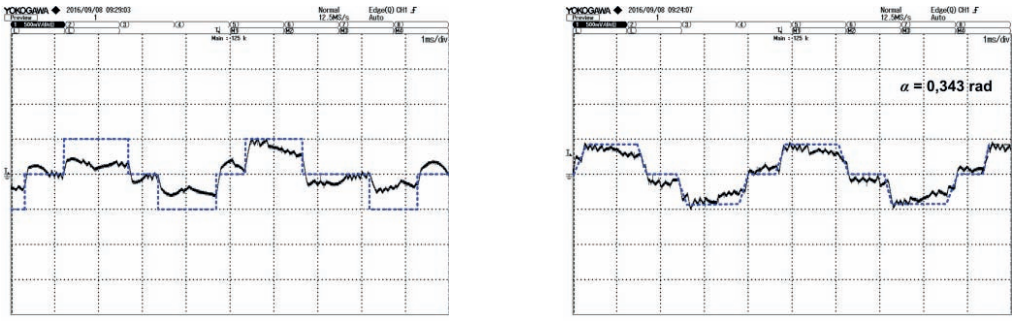

(a)

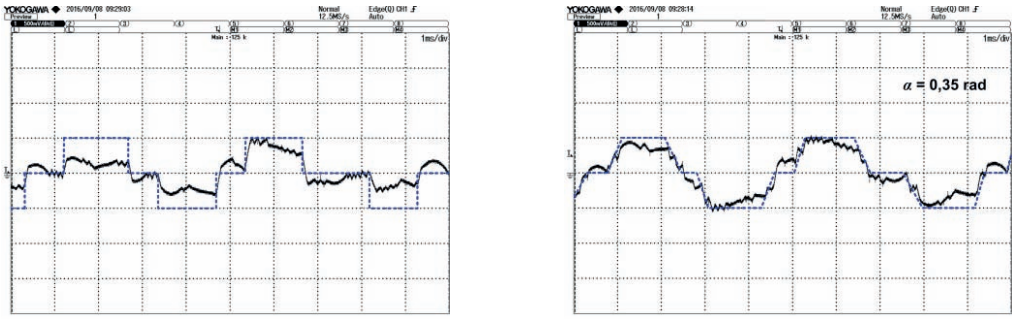

(b)

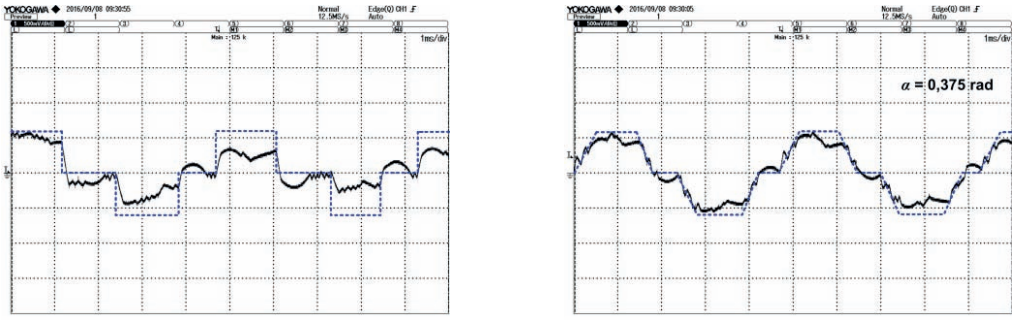

(c)

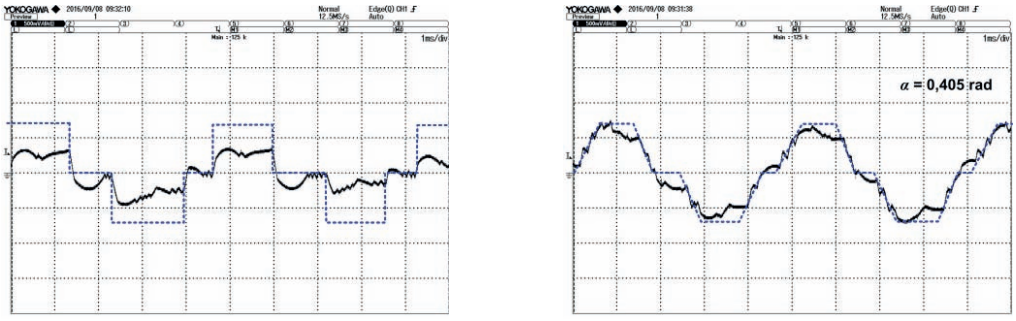

(d)

Figure 12. Experimental results of phase a motor current waveforms at 3250 rpm and different current commands: (a) $I = 4$ A, (b) $I = 5$ A, (c) $I = 6$ A, (d) $I = 7$ A.

at 4 A due to the decreased rms value of quasitrapezoidal motor current. However, the difference in power can easily be compensated by increasing the current command. Since every piece of equipment in our experimental set including the power inverter, BLDCM, and DC generator has power losses that we do not know exactly for each, the overall system efficiency is found to be around 50%, as shown in Figure 13c. Despite falling beyond the scope of this article, we expect that conduction losses of the inverter become dominant with respect to the switching losses under saturated-regulator operation as the switch operation is at its minimum value due to the high rotor speed. When making an efficiency comparison between the classical and presented method, it is remarkable to see that the presented technique does not give rise to serious decline in the overall efficiency while increasing the motor output power.

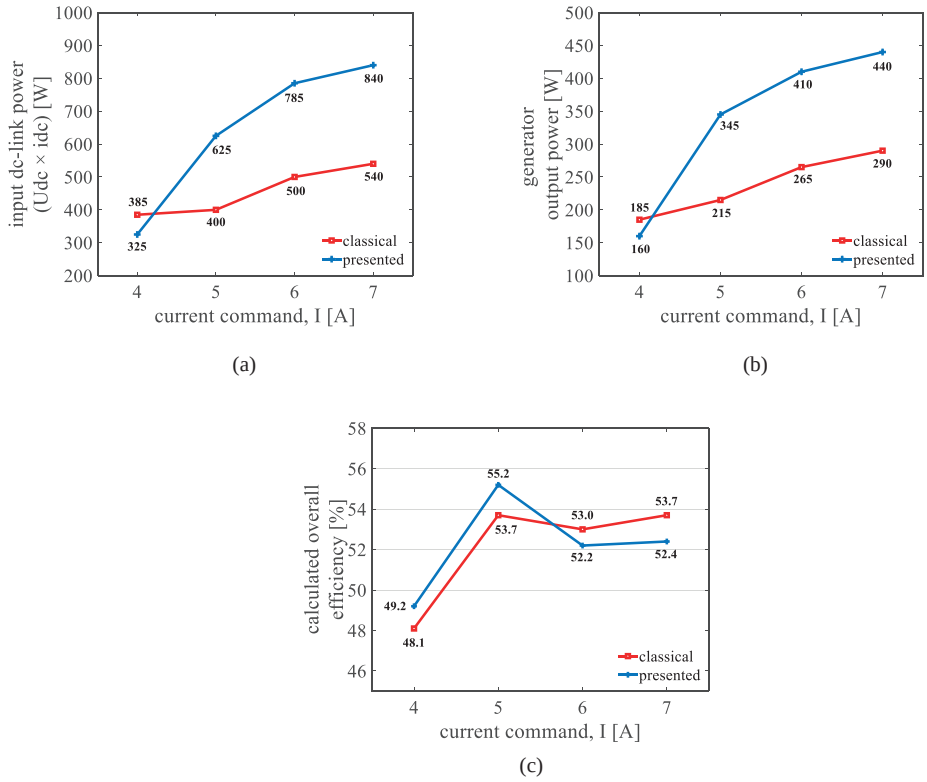

Figure 13. Measured power and efficiency results: (a) input DC-link power, (b) generator output power, (c) calculated overall efficiency.

5. Conclusions

Considering the idea of optimizing current slew rates of commutated phases to attenuate the saturated-regulator operation effect of a BLDCM through the poor current regulation in the face of large back emf, this paper presents a new reference current generation technique based on a simple FLE. After the reference currents are obtained in a shape similar to a trapezoid using θ_r, I, and the introduced α, motor currents are forced to follow the commanded currents by a standard hysteresis current controller. When the motor is excited by these current wave shapes, it is seen that the effect of the inverter saturation problem is attenuated, and this improvement has led to considerable increase in output motor power. The following list is given to provide a summarized exposition of the article's main results and the experimental concerns of the presented technique:

1) At 1000 rpm, the inverter saturation problem does not exist and the presented technique controls the motor with almost rectangular currents like the classical method in Figure 11. This is accomplished by the very small commutation angle.

2) Proportionally to the value of speed and to the current command, FLE sets α to its required value, which provides the ability for the reference currents to shift between rectangular shape and trapezoidal shape.

3) At a high speed of 3250 rpm above base speed, current regulators in the classical method are not active, and the deviation from the reference currents is dramatic. Under identical conditions, current tracking performance of the presented method is found to be clearly better, as shown in Figure 12.

4) Since the torque of a BLDCM is only proportional to phase current amplitude while the phase current and the back emf are in phase, we actually keep the torque production roughly constant by maintaining the phase current closer to its commanded value as speed increases. That is, the constant torque region of the motor is expanded to higher speeds in the study, which accordingly leads to develop more power than can be developed at base speed.

5) While operating at 3250 rpm and $I = 7$ A, the example motor is able to deliver 1.17 times greater power compared to its rated power, which proves the previous claim.

6) The control software complexity is just increased by the FLE integration, and no increase is introduced in terms of hardware requirement. Only the Hall sensors in the classical approach must now be replaced by an encoder to provide the increased resolution required by the current references shown in Figure 4.

7) We expect the conduction losses of the inverter to become dominant over the switching losses in both two approaches under saturated-regulator operation since the inverter switches in this case are almost in their ON state rather than being switched. In the classical technique, each power device is conducting during the entire 120°interval without experiencing PWM application, whereas the switching operation in our proposal is made to continue to some extent, which can be proven by analyzing the presented technique-based current waveforms closer to the commanded ones in Figure 12.

8) Though the expanded constant torque region is achieved, it is not possible to maintain motoring operation at very high speeds because the study focuses on keeping the current and back emf in phase to ensure the highest torque per current operation and output torque smoothness.

9) As the switching frequency tends to decrease at high rotor speeds owing to insufficient feed voltage between inverter voltage and motor emf, the current loop speed should be fast enough to force the current to track the commanded as much as possible.

10) Selections of current bandwidth and dead time should not be in larger values, which otherwise deteriorate the current control performance.

11) Improving the estimation performance of the critical variable α using any other soft computing techniques such as neural networks, ANFIS, and type-2 FL models may be contemplated as future studies at the expense of increased computational burden in comparison with the simple FLE.

Acknowledgments

The authors wish to express their genuine thanks to the reviewers and the editor for the critical review and observations that have proved to be an extensive help, contributing to substantially increase the quality of the paper in every round of the review process. The authors are also thankful to the Scientific and Technological Research Council of Turkey for having supported this work [TÜBİTAK, Grant Number 115E685].

References

[1] Türker T, Khudhair IOK. A switched current controller with commutation delay compensation for the reduction of commutation torque ripple in BLDCM drives. Turk J Elec Eng & Comp Sci 2017; 25: 2635-2646.

[2] Amirthalingam R, Mahadevan B. A new approach for minimizing torque ripple in a BLDC motor drive with a front end IDO dc-dc converter. Turk J Elec Eng & Comp Sci 2017; 25: 2910-2921.

[3] Viswanathan V, Jeevananthan S. Approach for torque ripple reduction for brushless DC motor based on three-level neutral-point-clamped inverter with DC-DC converter. IET Power Elec 2016; 8: 47-55.

[4] Shanthamoorthy V, Jothi Swaroopan NM. Design of intelligent controller to reduce the torque ripple in a brushless DC motor drive. International Journal of Advanced Research in Electrical, Electronics and Instrumentation Engineering 2014; 3: 467-476.

[5] Xinxin S, Siqin C. Commutation force ripple reduction in a novel linear brushless DC actuator based on predictive current control. Electr Pow Compo Sys 2011; 39: 1609-1620.

[6] Guanxiong L, Jinglin L, Shuaifu W. Investigation on leading angle flux weakening control of brushless DC motor. In: International Conference on Measuring Technology and Mechatronics Automation; 13–14 March 2010; Changsha, China. pp. 524-527.

[7] Bozhko S, Rashed M, Yeoh, SS, Yang T, Hill C. Flux weakening control of permanent magnet machine based aircraft electric starter-generator. In: 8th IET International Conference on Power Electronics, Machines and Drives; 19–21 April 2016; Glasgow, UK. pp. 1-6.

[8] Yin S, Wang W. Study on the flux-weakening capability of permanent magnet synchronous motor for electric vehicle. Mechatronics 2016; 38: 115-120.

[9] Chaithongsuk S, Nahid-Mobarakeh B, Caron JP, Takorabet N, Meibody-Tabar F. Optimal design of permanent magnet motors to improve field-weakening performances in variable speed drives. IEEE T Ind Electron 2012; 59: 2484-2494.

[10] Jahns TM. Torque production in permanent-magnet synchronous motor drives with rectangular current excitation. IEEE T Ind Appl 1984; 20: 803-813.

[11] Lawler JS, Bailey JM, McKeever JW, Pinto J. Extending the constant power speed range of the brushless DC motor through dual-mode inverter control. IEEE T Power Electron 2004; 19: 783-792.

[12] Atiq S, Lipo TA, Kwon BI. Experimental verification of winding switching technique to enhance maximum speed operation of surface mounted permanent magnet machines. IET Electr Power Appl 2016; 10: 294-303.

[13] Hemmati S, Lipo TA. Field weakening of a surface-mounted permanent magnet motor by winding switching. Electr Pow Compo Sys 2013; 41: 1213-1222.

[14] Ahmed H, Rajoriya A. A hybrid of sliding mode control and fuzzy logic control using a fuzzy supervisory switched system for DC motor speed control. Turk J Elec Eng & Comp Sci 2017; 25: 1993-2004.

[15] Karami MM, Itami A. Implementation of SVC based on grey theory and fuzzy logic to improve LVRT capability of wind distributed generations. Turk J Elec Eng & Comp Sci 2017; 25: 422-433.

[16] Rubiyah Y, Ribhan Z, Abdul R, Marzuki K, Ibrahim MF. Optimization of fuzzy model using genetic algorithm for process control application. J Frankl Inst 2011; 348: 1717-1737.

[17] Alpman E. Multiobjective aerodynamic optimization of a microscale ducted wind turbine using a genetic algorithm. Turk J Elec Eng & Comp Sci 2018; 26: 618-629.

[18] Tuncer A, Yıldırım M. Design and implementation of a genetic algorithm IP core on an FPGA for path planning of mobile robots. Turk J Elec Eng & Comp Sci 2016; 24: 5055-5067.

[19] Dao T, Wang Y, Nguyen N. Applying metaheuristic optimization methods to design novel adaptive PI-type fuzzy logic controllers for load-frequency control in a large-scale power grid. Turk J Elec Eng & Comp Sci 2016; 24: 4900-4914.

[20] Travis ML, Aruldoss M, Venkatasamy PV. A genetic bankrupt ratio analysis tool using a genetic algorithm to identify influencing financial ratios. IEEE T Evol Computat 2016; 20: 38-51.

[21] Suganthi L, Iniyan S, Samuel AA. Applications of fuzzy logic in renewable energy systems – A review. Renew Sust Energ Rev 2015; 48: 585-607.

[22] Kumar A, Kumar V. Evolving an interval type-2 fuzzy PID controller for the redundant robotic manipulator. Expert Syst Appl 2017; 73: 161-177.

[23] Kumbasar T, Hagras H. Big bang–big crunch optimization based interval type-2 fuzzy PID cascade controller design strategy. Inf Sci 2014; 282: 277-295.

[24] Öztürk N, Çelik E. An educational tool for the genetic algorithm-based fuzzy logic controller of a permanent magnet synchronous motor drive. Int J Elec Eng Educ 2014; 51: 218-231.

Appendix

```
//header files to be added
//some other standard codes to initialize DSP
void main(void){
float32 rules[5][5]={{30*pi/180,     8.25pi/180,   pi/180,        30pi/180,
      8.25*pi/180},
                     {22.75*pi/180,  pi/180,       pi/180,        8.25*pi/180,
               15.5*pi/180},
                     {8.25*pi/180,   pi/180,       8.25pi/180,    pi/180,
      8.25*pi/180},
                     {15.5*pi/180,   8.25*pi/180,  pi/180,        pi/180,
      22.75*pi/180},
                     {8.25*pi/180,   30pi/180,     pi/180,        8.25*pi/180,    30pi/180}};
//Initial variable values
pole_pairs=4;
mech_scaler=10000;
current_scalar=0.005;
hba=0.115;              //half of hysteresis current bandwidth
I=3.25;                 //can take values of 3,4,5,6, and 7Amper
//Configure ePWM6 signal for ADC
EPwm6Regs.TBPRD=999;    //Set period for ePWM6 to 75khz for ADC, TBCLK=150Mhz/1x2
//Configure ePWM1 signal for FLE
EPwm1Regs.TBCTL.bit.CLKDIV=3;
EPwm1Regs.TBPRD=46874;  //Set period for ePWM1 to 200khz for FLE, TBCLK=150Mhz/8x2
//Configure CPU-Timer 0 to interrupt every 10000usecond(100hz) for speed calculation
ConfigCpuTimer(&CpuTimer0,150,10000);

for(;;){
     position=EQep1Regs.QPOSCNT;
     direction=EQep1Regs.QEPSTS.bit.QDF;
     theta_mech=(float32)2*pi*position/mech_scaler;
     theta_elec=pole_pairs*theta_mech;
     tetaref=fmod(theta_elec,2*pi);      //tetaref in the range [0, 2*pi]
     //codes to generate quasi-trapezoidal current references given in Table 1
     } //end for
} //end main
interrupt void adc_isr(void)     //ADC interrupt given for ia
{
     adc1=AdcRegs.ADCRESULT0>>4;
     adc1-=2048;
     ia=adc1*current_scalar;
     iae=iaref-ia;

     //phase a
     if(iae>=hba)
     {
      GpioDataRegs.GPBCLEAR.bit.GPIO62=1;
      DELAY_US(7);       // dead time in us
      GpioDataRegs.GPBSET.bit.GPIO63=1;
     }
     else if(iae<=-hba)
     {
      GpioDataRegs.GPBCLEAR.bit.GPIO63=1;
      DELAY_US(7);       // dead time in us
      GpioDataRegs.GPBSET.bit.GPIO62=1;
     }
}
interrupt void fuzzy_estimator(void)
{
  //codes to realize fuzzy logic estimator which is widely illustrated in above sections
}
interrupt void cpu_timer_0(void)
{
```

```
  //codes for motor speed measurement
}
void EQep1_Init(void)
{
  /*codes for Enhanced Quadrature Encoder Pulse (eQEP) Module which can be found in the manual
document SPRUG05A.pdf*/
}
void Gpio_setup(void)
{
  /*codes for adjusting the registers of General-Purpose Input/Output (GPIO) Module used in
the algorithm. For more information, refer to manual document SPRUFB0D.pdf*/
}// No more.
```